Molecular tagging velocimetry in turbulence using biacetyl

M. Mirzaei
Institute for Molecules and Materials, Radboud University of Nijmegen, PO Box 9010/51, 6500 GL Nijmegen, The Netherlands

N. J. Dam*
Mechanical Engineering Department, Eindhoven University of Technology, PO Box 513, 5600 MB Eindhoven, The Netherlands

W. van de Water
Physics Department, Eindhoven University of Technology, PO Box 513, 5600 MB Eindhoven, The Netherlands

(Received 12 July 2012; revised manuscript received 6 September 2012; published 19 October 2012)

We evaluate various molecular tagging velocimetry (MTV) techniques for application in turbulent flows of gases where the smallest length scales must be resolved. We argue that tracer diffusion dictates the use of large complex molecules and discuss a few candidate molecules. The accuracy of MTV is determined by the profile of written lines which widen due to molecular dynamics, including both diffusion and chemical reaction. We evaluate these profiles for tagging with phosphorescing biacetyl molecules, which is a commonly used probe in MTV. For relatively large laser power, these profiles are determined not by molecular diffusion, but by the triplet-triplet annihilation reaction of excited biacetyl molecules. We identify a new reaction pathway, and present a model for the observed line shapes. The rapid widening of tagged lines of biacetyl molecules due to chemical reaction restricts this MTV technique to large-scale turbulent motion in gases of comparable molecular weight.

DOI: 10.1103/PhysRevE.86.046318 PACS number(s): 47.80.Cb, 34.50.Rk, 42.62.−b

I. INTRODUCTION

In molecular tagging velocimetry of a gas, the molecules of the gas itself are used as flow tracer, in contrast to other techniques where the flow must be seeded with particles acting as tracers. These particles may be too large or too heavy to follow the rapid changes of the velocity; they may not reach everywhere in the flow, while their density is too small to resolve velocity differences across very small distances, as would be needed in turbulent flow.

Molecules can be tagged by exciting them with laser light to a long-lived metastable, or phosphorescent, state. Stable molecules may also be created from others, and visualized with laser light. In this way, these tracers can be created at will, overcoming the drawbacks of particle tracers that must be sown in the gas. Molecular tagging velocimetry (MTV) has found widespread application, both in liquids and gases [1]. In this paper we focus on the ability of MTV to resolve the smallest length (and velocity) scales in a turbulent flow of a gas. In order to measure this small-scale motion, for example to directly infer Reynolds stresses from velocity gradients, the application of MTV must meet the requirements of temporal and spatial resolution of the smallest turbulence time and length scales. Time scales are important for unstable tagged molecules, whereas length scales are associated with optics, but also with molecular dynamics, as molecules of a gas do not necessarily follow the velocity field of the flow.

In this paper we will first set the scales by listing the properties of three well-documented turbulent flows that can be created in the laboratory. Next we will briefly review three MTV techniques and contrast their properties with the time and length scales of these turbulent flows. It will turn out that an important length scale of MTV is associated with molecular diffusion. Large complex molecules have an advantage as they diffuse slowly and follow the velocity field more faithfully. An excellent candidate would be biacetyl, which has a relatively large molecular weight. In Sec. IV we will describe experiments to determine the accuracy of MTV using biacetyl molecules, but argue that length scales of MTV with these tracers are not determined by diffusion, but by chemical reaction, and document a different reaction pathway in addition to the ones already known.

Molecular tagging velocimetry in air, based on a metastable state of oxygen, was introduced by Miles and co-workers [2–5], and is also known as Raman excitation plus laser-induced electronic fluorescence (RELIEF). In RELIEF, vibrationally excited oxygen is created by stimulated Raman scattering. Due to its long lifetime it can be excited at adjustable later times to an excited electronic state, the relaxation of which is an emissive process and can be interrogated. The requirement of three frequencies (i.e., two for tagging and one to interrogate) makes RELIEF one of the most sophisticated MTV techniques. It has been successfully used to measure high-order statistical properties of a turbulent flow of air [5].

The tracer molecule NO, which is not normally present in air, can be produced in several different ways: by dissociating NO_2 molecules in the focus of a 308-nm XeCl excimer laser [6], by dissociation of tert-butyl nitrite [7], or by irradiating air with an intense ArF laser beam. The latter is known under the acronym of APART (air photolysis and recombination tracking), and has been developed in our group over the last ten years [8–11]. This stable tracer can be followed by laser-induced fluorescence. Therefore, this technique needs two lasers, one for writing, and one for reading.

When the tracer is phosphorescent, a single laser suffices for the excitation and the image can be detected by directly monitoring the long-lived luminescence from the tracer upon

*Corresponding author: n.j.dam@tue.nl

its radiative return to its ground state. The tracer may be re-excited, and thus is reusable, however, the limited luminescence lifetime forms a serious restriction for turbulence measurements. In Sec. III we will review MTV with biacetyl, a popular phosphorescent tracer [12–16].

A disadvantage of metastable and luminescent tracers is reactive collisions with each other or with other molecules, quenching the excited state. In fact, quenching is an issue pervading most measurements, and the most problematic quencher in engineering applications is oxygen. Although one can make unquenchable tracers by connecting small molecular subunits for liquid-phase flow diagnostics [17–19], when it comes to gas-phase flow diagnostics, the number of possible suitable candidate shrinks dramatically. Among these candidates, biacetyl and acetone are two famous and more applicable ones; in this paper we will focus on biacetyl.

II. MTV IN TURBULENT FLOWS

The resolution of the smallest length and time scales in turbulence imposes restrictions on the application of molecular tagging velocimetry. In this section we will contrast the length and time scales of MTV with those of a few common turbulent flows that can be created in the laboratory. The time scale of MTV is the lifetime of the tagged molecule, while its length scale is the distance over which a tagged molecule straggles during a turbulence time. It will turn out that the latter length scale, which is often overlooked, is essential for the application of MTV in turbulent flows.

In turbulence velocimetry, the typical interest will be in the statistical properties of the small-scale motion, such as the small-scale gradients and the Reynolds stresses. The smallest relevant length scale is the Kolmogorov length η and the smallest relevant time scale is the Kolmogorov time τ_η. In the cascade picture of turbulence, the energy input ϵ per unit mass is transported to smaller and smaller scales, until the length scale becomes so small that viscous dissipation takes over. Therefore, η and τ_η follow from ϵ and the kinematic viscosity ν as $\eta = \nu^{3/4}\,\epsilon^{-1/4}$ and $\tau_\eta = \nu^{1/2}\,\epsilon^{-1/2}$. To measure gradients of the velocity field, the spatial resolution should match η, while velocities are deduced from displacements of tagged molecules during τ_η. The measurement of displacement in times smaller than τ_η suffers from an unnecessary loss of accuracy.

Experimentally, we will consider typical cases in which a tracer distribution is created by one or more laser beams, and visualized with an (intensified) charge-coupled device (CCD) camera. In the case of luminescent tracers, the exposure time t_e should be long to maximize the number of collected photons, but short enough to prevent motion unsharpness. Motion unsharpness is determined by the large-scale velocity. Turbulent flow with root-mean-square velocity u may or may not have a mean velocity U. To make our argument quantitative, we shall consider turbulent flows with $U/u \gg 1, U/u \gtrsim 1$, and $U = 0$.

Table I lists three typical turbulent flows of air which are used commonly in fundamental studies of turbulence, namely turbulent flow in a wind tunnel generated by an active grid [20], turbulence created by a jet [11], and finally turbulence with $U = 0$, generated acoustically using loudspeakers [21].

Let us now contrast the time and length scales of MTV with those of Table I. First, in order to deduce small-scale velocities from small-scale displacements, the phosphorescence time $t_{\rm phos}$ should be larger than the Kolmogorov time τ_η. Second, the exposure time should be small such as to prevent motion unsharpness. Specifically, a tracer should move over less than a Kolmogorov scale η during the exposure time. For flows with a mean velocity this implies $t_e \lesssim \eta/U$, while for flow without a mean velocity, the exposure time should satisfy $t_e \lesssim \eta/u$.

In the RELIEF (metastable O_2) [2–5], and APART (NO) [8–11] techniques, the writing and reading steps are both essentially instantaneous, so that restrictions on t_e related to motion unsharpness do not exist. Moreover, the lifetime of NO tracers is very long, much longer than the Kolmogorov time of each of the flows in Table I. Contrary to the NO technique, the metastable O_2 molecules of the RELIEF technique are fragile with lifetimes determined by the vapor pressure of water; in saturated air at room temperature the lifetime is a mere 6 μs [5], which makes them suitable for flow 1 only.

An example of a phosphorescent tracer is biacetyl [13,15,22]. The lifetime $t_{\rm phos}$ of the phosphorescence in an oxygen-free environment is $\mathcal{O}$(ms), so that these molecules can be used in turbulent flow 1 of Table I. Other turbulent flows have a too large Kolmogorov time. During the phosphorescence time, therefore, small–scale relative displacements of these molecules remain a fraction of the Kolmogorov length.

Starting from the condition in Table I, let us now study how our requirements change when flow parameters such as the mean velocity U, turbulent velocity u, or the size L of the experiment change. Therefore, we explicitly write the dependence of Re_λ, η, and τ_η on these parameters:

$$\mathrm{Re}_\lambda = L^{1/2}u^{1/2}15^{1/2}\nu^{-1/2}C_\epsilon^{-1/2}, \quad \eta = L^{1/4}u^{-3/4}\nu^{3/4}C_\epsilon^{-1/4},$$
$$\tau_\eta = L^{1/2}u^{-3/2}\nu^{1/2}C_\epsilon^{-1/2}.$$

where C_ϵ links large-scale motion to energy input, $\epsilon = C_\epsilon u^3/L$. This implies that the phosphorescence lifetime $t_{\rm phos}$ and exposure time t_e depend on the size L of the experiment (which we take to be the integral length scale) as $t_{\rm phos} \gtrsim \tau_\eta \propto L^{1/2}\,u^{-3/2}$, while for the exposure time $t_{\rm e}$ in turbulence

TABLE I. Characteristics of typical turbulent flows of air that can be realized in the laboratory: (1) turbulence in the efflux of a small jet [11], (2) turbulence in a wind tunnel driven by an active grid [20], (3) zero mean flow turbulence driven by synthetic jets [21]. All flows have a large enough Reynolds number and a sizable inertial range to display a Kolmogorov spectrum, $E(k) \sim k^{-5/3}$.

Flow	U (m s^{-1})	u (m s^{-1})	ε (m^2 s^{-3})	Re_λ	τ_η (s)	η (m)	t_e (s)
1	40	10	4.7×10^4	460	1.8×10^{-5}	1.7×10^{-5}	4×10^{-7}
2	14	1.4	15.3	473	9.6×10^{-4}	1.2×10^{-4}	8.6×10^{-6}
3	0	0.86	11.3	218	1.1×10^{-3}	1.3×10^{-4}	1.5×10^{-4}

without a mean velocity $t_e \lesssim \eta/u \propto L^{1/4}\, u^{-7/4}$, while for flows with a mean velocity $t_e \lesssim \eta/U \propto L^{1/4}\, u^{-3/4} U^{-1}$. These dependencies imply that for a given integral length scale L large turbulent velocities give short turbulence times, and many turnover times can be observed in a phosphorescence time. However, with increasing u, the exposure time, and thus the number of collected photons, decreases rapidly. If intensity is a problem, molecular tagging in turbulence with a large mean flow is problematic.

Imagine that we tag molecules along a focused laser beam. At first view, the smallest resolved length scale in MTV is determined by the width of the focus, while the largest length scale is set by the Rayleigh length. The width of a focus can easily match the smallest turbulent scales η in the wind tunnel (flow 2) and synthetic-jet driven (3) flows, but it is a challenge to focus down to the smallest length scale in the jet flow (1), $\eta = 15\ \mu$m. As will appear in this paper, more relevant length scales are set by the dynamics of the molecular tracers. This dynamical behavior involves molecular diffusion and chemical reactions.

Let us assume that a line of tagged molecules has a Gaussian cross section, with radial density $n(r) \propto \exp(-r^2/\sigma^2)$. If the width σ is smaller than the Kolmogorov scale η, the line will be wrinkled due to the turbulence, with the smallest wrinkles having size η. At the same time, this line will widen due to molecular diffusion,

$$\sigma^2(t) = \sigma^2(0) + 4Dt,$$

with D the diffusion coefficient. In MTV the tagged molecules diffuse into the gas of the untagged ones. If the tagged molecules have a similar weight and size as the other molecules, the diffusion D of mass approximately equals the diffusion ν of momentum (the kinematic viscosity); the ratio $\nu/D = \mathrm{Sc}$ is the Schmidt number. A Schmidt number of order unity has a remarkable consequence for the observability of the smallest eddies in turbulence: the smallest turbulent wrinkles will always be blurred by diffusion. This follows from the growth of σ during one small-eddy turnover time τ_η, starting from a line of zero width,

$$\begin{aligned}\sigma(\tau_\eta) &= (4D\tau_\eta)^{1/2} = (4\nu \mathrm{Sc}^{-1}\tau_\eta)^{1/2} \\ &= [4\nu \mathrm{Sc}^{-1}(\nu/\epsilon)^{1/2}]^{1/2} = 2\eta \mathrm{Sc}^{-1/2}.\end{aligned}$$

This fundamental restriction calls for the use of complex (large) molecules that have large Schmidt numbers for molecular tagging velocimetry in turbulent flows. In the next section we will discuss one such candidate molecule, biacetyl, and study the widening of lines of excited biacetyl molecules in Secs. V and VI.

III. BIACETYL MOLECULE

Biacetyl has always received a lot of attention because of its phosphorescence in the gas, liquid, and solid phases [23,24]. It also has a relatively low triplet energy (about 20 000 cm^{-1}) [25], which makes it a suitable candidate for triplet energy transfer studies [26–28]. In fact, it has some unique properties that make it suitable for flow field diagnostics as well. It has a relatively high vapor pressure (5.3 kPa at room temperature) with no obvious condensation below 2.7 kPa [29], meaning that it can be easily added to the flow of a gas. It is nontoxic and commonly used as an additive in dairy products. Its continuous broad absorption band in the UV and visible range (250–470 nm) [15] makes it an easy candidate for laser-induced fluorescence (LIF) or laser-induced phosphorescence (LIP) techniques.

Two broad absorption maxima exist at $\lambda = 270$ nm and $\lambda = 420$ nm. Excitation occurs in the singlet system, but efficient intersystem crossing results in a large fraction of excited molecules ending up in the triplet manifold. From there, they can relax back to the (singlet) ground state by photon emission, but this is a slow process (phosphorescence) and the excited triplet states are susceptible to the environment through intermolecular collisions. Thus, the excitation of biacetyl leads to both fluorescence and phosphorescence emission. The phosphorescence lifetime of biacetyl is about 1.52 ms [27], but the observed lifetime can be (much) lower due to a variety of reasons. Specifically, oxygen molecules can easily interact with the excited biacetyl molecules and decrease the phosphorescence lifetime [13]. Consequently, it must be used in an O_2-free environment, and nitrogen is usually used as carrier gas. Due to the very short lifetime of the fluorescence emission ($\approx$10 ns), phosphorescence is the only process that can be used in most flow visualization experiments.

Almy and Anderson [30] were among the first to study the lifetime of biacetyl fluorescence experimentally. They also investigated the quenching of biacetyl by oxygen. Comprehensive studies on photochemical processes of biacetyl were done by the group of Noyes [31,32]. They looked at the detailed mechanism of the primary process and its relationship to the singlet and triplet excited states, which varies with wavelength [31] and temperature [32]. The triplet-triplet annihilation reaction in biacetyl vapor was studied by Garabedian and Doms through the pressure dependence of the phosphorescence, which revealed a bimolecular quenching of the lowest triplet state [25]. The lifetime of the excited biacetyl triplet and first-excited singlet molecules in vapor phase experiments was studied in Ref. [27].

Finally, the excitation intensity dependence of the triplet-triplet annihilation reaction at 436.5 nm has the consequence that the rates of phosphorescence decay in experiments at high intensity deviate markedly from the rates observed at low intensities [28].

Molecular tagging measurements using biacetyl laser-induced fluorescence or phosphorescence has been suggested for visualizing structures and measuring velocity of flows by Epstein who used biacetyl as a tracer to measure the three-dimensional density distribution in a transonic compressor rotor [12]. McKenzie *et al.* demonstrated a laser-induced fluorescence technique for measuring relative time-dependent density fluctuations [29]. Jian-Bang and co-workers proposed a method for measuring the density, temperature, and velocity of N_2 gas flow by laser-induced biacetyl phosphorescence [16,22]. Based on their studies, Hu and co-workers performed instantaneous, quantitative, planar measurements of fluid mixed at the molecular level, using biacetyl fluorescence and phosphorescence emission [14,15].

Molecular tagging velocimetry using phosphorescent biacetyl molecules has been successfully tried in turbulent plane Couette-Poiseuille flows of N_2 gas by Thurlow and

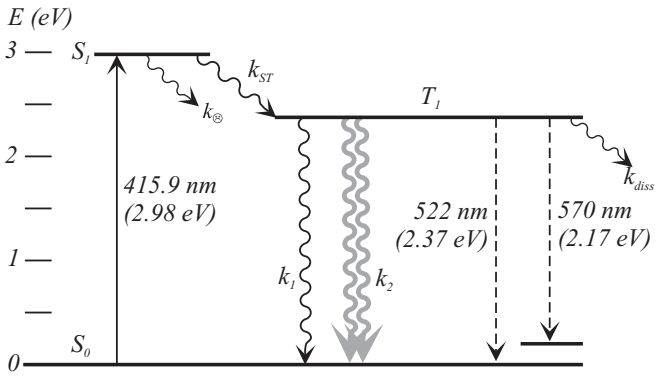

FIG. 1. Schematic view of the energy levels of biacetyl. The excitation by 415.9-nm photons reaches the singlet level, which relaxes to the lowest triplet state T_1 through intersystem crossing. This state emits light, with lifetime determined by k_1 and triplet-triplet annihilation (k_2). The rate of deexcitation through collisions with other molecules is k_{diss}.

Klewicki [33]. Since the widths of the written lines were an order of magnitude larger than the smallest turbulent length scale, reported Reynolds stresses were not measured directly, but inferred from a momentum balance involving mean quantities. Similar to those of the present paper, their linewidths are ≈600 μm, with the position accuracy enhanced using image processing techniques [34].

The light-induced reaction pathways of biacetyl which are relevant for flow-field diagnostics are summarized in the following equations:

$$\text{Bi} + h\nu \rightarrow {}^1\text{Bi}, \tag{1a}$$

$${}^1\text{Bi} \rightarrow {}^3\text{Bi}, \tag{1b}$$

$${}^3\text{Bi} \rightarrow \text{Bi} + h\nu_{\text{phos}}, \tag{1c}$$

$${}^3\text{Bi} + M \rightarrow \text{Bi}, \tag{1d}$$

$${}^3\text{Bi} + {}^3\text{Bi} \rightarrow \text{Bi}^* + \text{Bi}, \tag{1e}$$

$${}^3\text{Bi} + \text{Bi}^* \rightarrow \text{Bi} + M, \tag{1f}$$

in which Bi is a ground-state molecule, ^{3}Bi is the first-excited triplet biacetyl molecule and M is another molecular species. Since the ratio of phosphorescence to fluorescence yield is about 60 : 1 [35], we have neglected the vibrationally excited singlet-state biacetyl i.e., ${}^1\text{Bi} \rightarrow \text{Bi} + h\nu_{\text{flu}}$. As the vibrational relaxation is very efficient and fast compared to the phosphorescence process, we neglected it as well. In fact, we assumed that every act of absorption leads to a triplet biacetyl molecule in its ground vibrational state through reactions Eqs. (1a) and (1b). A schematic view of the energy levels of the biacetyl molecules is shown in Fig. 1.

IV. EXPERIMENT

Biacetyl was excited at wavelength $\lambda = 415.9$ nm, where it has a large absorption peak. Light with this wavelength was created starting from the third harmonic $\lambda = 355$ nm output of a pulsed Nd:YAG laser (Quanta-Ray, SPECTRA-Pro 250-10) which was subsequently shifted to $\lambda = 415.9$ nm using stimulated Raman scattering (SRS) in a high-pressure (0.8 MPa) hydrogen cell. A schematic view of the experiment is shown in

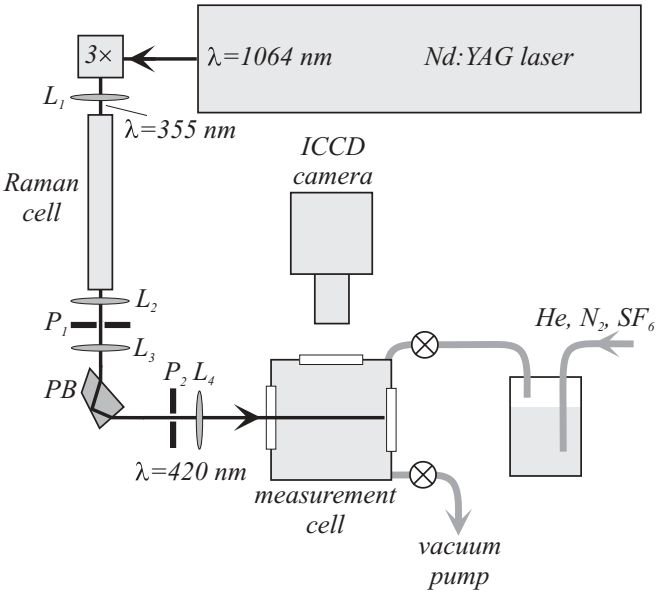

FIG. 2. Schematic view of the experimental setup. The lenses L_3 (focal length $f_3 = 70$ mm) and L_4 ($f_4 = 30$ mm) form a telescope; the lens L_5 ($f_5 = 50$ mm) further shapes the beam inside the measurement cell. A Pellin-Broca prism (PB) was used to separate SRS wavelengths.

Fig. 2. To increase the efficiency of the frequency conversion, we used a positive lens with focal length $f_1 = 600$ mm before the hydrogen cell to focus the pump beam. Another positive lens with approximately the same focal length ($f_2 = 500$ mm) was used to collimate the frequency-converted beam. The beam exiting the Raman cell was further shaped using a telescope consisting of a combination of two positive lenses and a pinhole. The Raman cell produces several Stokes orders, which were separated using a Pellin-Broca prism. The desired first Stokes beam ($\lambda = 415.9$ nm) was then selected using a diaphragm. An extra positive lens ($f_5 = 50$ mm) was used immediately before the measurement cell to focus this beam.

Since our interest is in the evolution of tagged line shapes, our experiments were performed in still gas in a cell. The experimental setup is sketched in Fig. 2. We used a bubbler to saturate the He, N_2, and SF_6 carrier gases with biacetyl. The measurement cell was a black anodized aluminium cylinder with three windows, two for the entrance and exit of the laser beam and one for detection. Since very small amounts of oxygen would quench the phosphorescence, the measurement cell was evacuated to about 10 Pa (10^{-4} bars). To minimize the oxygen quenching effect, the measurement cell was flushed with the mixture of biacetyl-carrier gas several times before the experiment. Phosphorescence was detected with an intensified charge-coupled device (ICCD) camera (Princeton Instruments PIMAX 2). A custom lens (Bernhard Halle Nachfl) was used with a fixed focus of 250 mm and $f/2.5$. The 1024×1024 pixel camera image corresponded to an area of 9.3×9.3 mm^2 in the object plane. A digital delay generator (SRS DG 535) provided the required delay t between the Nd:YAG laser and the ICCD camera. As we tagged lines in still gas, an average over images could be done to increase the signal-to-noise ratio. In addition, the exposure time t_e was increased with increasing delay time t, such that

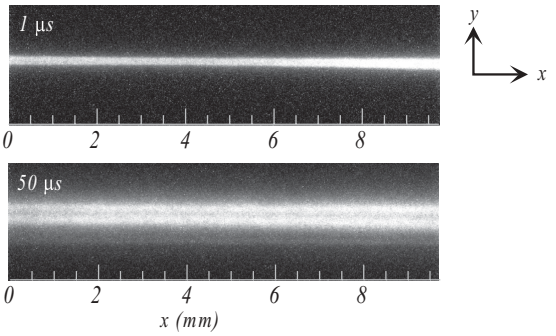

FIG. 3. Phosphorescing lines of triplet biacetyl molecules in still SF_6 carrier gas at 1 bar for two delay times since excitation of the triplet molecules. At $t = 50\ \mu$s after creation, the line has widened considerably. The broadening, and the slight depression of the concentration in the center are due to the triplet-triplet annihilation reaction. The intensity scales have been normalized.

$t_e = t/10$. This approximately compensated for the decrease of the phosphorescence signal with increasing delay time t, which ranged $t = 0.5$–$500\ \mu$s.

V. EXPERIMENTAL RESULTS

The absolute initial number of triplet biacetyl molecules is not known precisely in our experiments. It is determined by the vapor pressure of the ground-state molecules, the energy of the 420-nm laser pulse, and the absorption length of the laser light. At ambient temperature $T = 300$ K the vapor pressure of biacetyl molecules corresponds to a gas-phase density of $1.3 \times 10^{24}\ \mathrm{m}^{-3}$, but we do not know the concentration after the bubbling system. Therefore, we will choose a value of n_0 that fits the cross section of the tagged line.

In order to test the influence of the ambient gas on the evolution of the line shape, tagged lines of triplet biacetyl molecules were written in He, N_2, and SF_6 carrier gases at pressures of 0.5 and 1 bar. Two types of experiments were done: experiments in which the laser pulse energies were large enough for the TTA process to be relevant ("high" power), and experiments at very small pulse energies ("low" power) to measure the widening of lines due to molecular diffusion only.

Typical lines of tagged molecules at two different delay times are shown in Fig. 3. The carrier gas of these lines was SF_6 at 1 bar. At the smaller delay time we essentially probe the profile of the excitation beam through fluorescence; at larger times the width of the lines rapidly increases while the line profiles develop a dip in the center. The intensity scales of Fig. 3 have been normalized, and because the decay of the intensity depends quadratically on the density, the high-density line center decays more rapidly than the line wings, resulting in an apparent line widening. A similar behavior is found at a pressure of 1 bar, and in other carrier gases, but the central dip in the line profile in He carrier gas is smallest.

The evolution of the observed line profiles is shown in Fig. 4. As demonstrated in Fig. 4(a), the fluorescence at zero time delay can in this case be represented well by a Lorentzian profile, $I_y(y) = (\pi\sigma)^{-1}[1 + (y - y_0)^2/\sigma^2]^{-1}$, where σ is the linewidth and y_0 is the line center. The evolution of the dip in the line center can be clearly seen. We will argue below

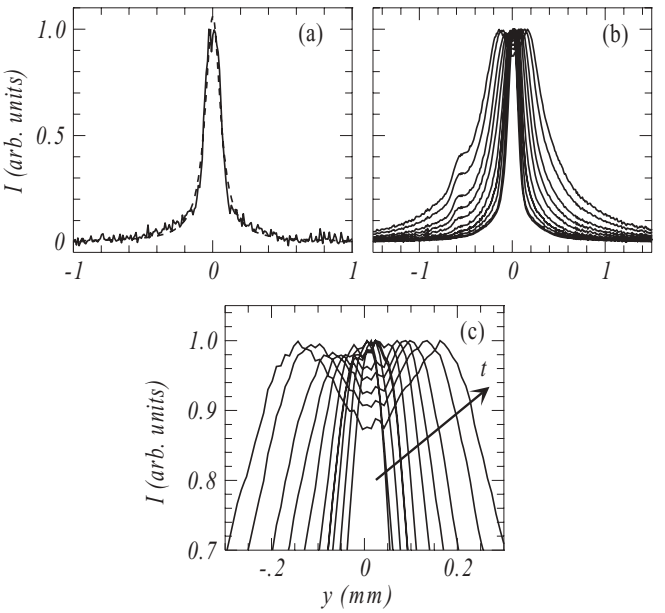

FIG. 4. Line profiles $I_y(y)$ of phosphorescent biacetyl molecules measured in SF_6 gas at 0.5 bar. (a) At time delay $t = 0$, full lines shows the data, dashed line a fit of a Lorentz profile, $I_y(y) = (\pi\sigma)^{-1}(1 + y^2/\sigma^2)^{-1}$, with $\sigma = 6.5 \times 10^{-5}$ m. (b) Profiles at increasing time delays, $t = 0, 0.2, 0.5, 1, 2, 5, 10, 20, 50$, and $100\ \mu$s. (c) Enlargement of the central region; the arrow points to increasing delay time. The profiles have been normalized so that their maximum is 1.

that this feature is due to a new quenching process of excited biacetyl molecules, thus revealing yet unknown details of the chemistry of triplet molecules.

The squared half maximum width increment Δ^2 of a Gaussian line grows diffusively as $\Delta^2(t) = \sigma_{1/2}^2(t) - \sigma_{1/2}^2(0) = 16\ln(2)Dt$, with D the molecular diffusion coefficient, and $\sigma_{1/2}$ the full linewidth at half maximum. From now on we will characterize the widening of tagged biacetyl lines using $\Delta^2(t)$. Figure 5 shows $\Delta^2(t)$ for all our experiments at relatively large laser pulse energies in He, N_2, and SF_6 carrier gas at 0.5 and 1 bar. All curves approximately collapse, which indicates that line widening is not influenced by the carrier

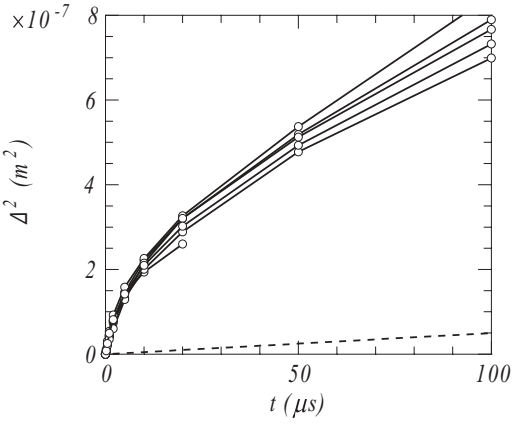

FIG. 5. Time dependence of full width half maximum increment Δ^2. Triplet-biacetyl lines were written in He, N_2, and SF_6 buffer gases at pressures of 0.5 and 1 bar. The dashed line indicates the line widening due to molecular diffusion in the 0.5-bar He carrier gas.

gas, but by interaction among biacetyl molecules only. At large times, the rise of $\Delta^2(t)$ is much faster than that of molecular diffusion, which would be fastest in the low-pressure He gas. This asymptote is included in Fig. 5. We will now analyze the dynamical behavior of the profiles in terms of reaction equations for the triplet molecular density [Eq. (1)].

VI. ANALYSIS

According to the processes Eqs. (1c), (1d), and (1e), in which the excited triplet density decays due to radiation, collisions with other molecules M and triplet molecules ^{3}Bi, the time-dependent radial concentration of biacetyl molecules should be described by

$$\frac{\partial \theta_B}{\partial t} = -k_1\theta_B - k_2\theta_B^2 + D\nabla^2\theta_B, \tag{2}$$

where k_1 is the rate constant of linear decay, which includes radiation and quenching due to collisions with other molecules, such as oxygen. In an oxygen-free environment the lifetime of triplet molecules is $k_1^{-1} = 1.5$ ms, but k_1 rapidly increases with increasing oxygen concentration, $k_1 = (672 + 2.3 \times 10^2\ p_{O_2})\ s^{-1}$, with p_{O_2} the oxygen pressure in N m^{-2} [27].

The rate constant k_2 embodies the triplet-triplet annihilation reaction [Eq. (1d)]. Its value $k_2 = 1.39 \times 10^{-15}$ s^{-1} m^{-3} has been determined in Ref. [28] using an experimental technique similar to ours. The information used was the temporal decay of the integrated line intensity. Due to the quadratic dependence on the concentration, this technique needs accurate information on the line profile. The acoustic-optical technique in Ref. [36] yielded $k_2 = 7.6 \times 10^{-16}$ s^{-1} m^{-3}, which is approximately half that of Ref. [28]. Surprisingly, these values are larger than the hard-sphere molecular collision rate, which indicates that TTA collisions are relatively efficient. We conclude that k_2 is not known very well, and in this paper we take the value $k_2 = 1.39 \times 10^{-15}$ s^{-1} m^{-3}.

We assume that the initial density is normalized such that $\int_0^\infty \theta_B(r,t=0)\, 2\pi r\, dr = n_0$, the total number of excited triplet molecules per unit length along the laser beam. We also assume that the radial density profile $\theta_B(r,t)$ is proportional to the radial intensity profile $I_r(r,t)$. What is observed in the experiment is the chord-integrated intensity profile $I_y(y,t)$, which follows from the radial profile through the Abel transform

$$I_y(y) = \int_y^\infty \frac{I_r(r)}{(r^2 - y^2)^{1/2}} r\, dr.$$

The observed initial profile $I_y(y,t=0)$ is close to a Lorentzian [Fig. 4(a)], for which the inverse Abel transform can be done exactly, and

$$\theta_B(r,0) = \frac{n_0}{2\pi\sigma^2} \frac{1}{(1 + r^2/\sigma^2)^{3/2}}. \tag{3}$$

Starting from the initial profile, the time-dependent density profiles $\theta_B(r,t)$ can be computed, but to compare them to the observed line profiles, they must again be Abel transformed.

The last term on the right-hand side of Eq. (2) represents the effect of molecular diffusion, $D\nabla^2\theta_B = D\frac{1}{r}\frac{\partial}{\partial r}(r\frac{\partial\theta_B(r,t)}{\partial r})$. In absence of molecular diffusion, an ordinary differential equation results, with the analytic solution

$$\theta_B(r,t) = \frac{k_1\ \theta_B(r,0)\exp(-k_1 t)}{k_1 + k_2\theta_B(r,0)(1 - \exp(-k_1 t))}.$$

For long times, $t \gg k_1^{-1}$, the concentration is $\theta_B(r,t) = \exp(-k_1 t)/[k_2/k_1 + \theta_B(r,0)^{-1}]$, which becomes independent of the initial concentration, $\theta_B(r,t) = (k_1/k_2)\exp(-k_1 t)$, if the initial concentration is large, $\theta_B(r,0) \gg k_1/k_2$. In that case, there is an initial decay from the initial value, $d\theta_B/dt|_{t=0} \approx -k_1\, k_2\, \theta_B^2(r,0)$, which becomes steeper as the initial concentration increases. For short times, $t \ll k_1^{-1}$ and large initial concentration, $\theta_B(r,t) \sim t^{-1}$.

If the initial concentration $\theta_B(r,0)$ has a single maximum, as in our experiments, this first-order process cannot explain the observation of a dip growing in the center of the measured profile, and additional processes are needed. This conclusion remains unaltered when molecular diffusion is included, although an analytic solution of Eq. (2) is no longer possible.

In order to explain the dip growing into the central portion of the written line of phosphorescent biacetyl molecules, a mechanism that efficiently removes ^{3}Bi molecules in locations where they are abundant is required. We consider two such mechanisms, differing in the fate of the collision partners in ^{3}Bi-^{3}Bi collisions (the TTA events).

In the first case both collision partners end up in the ground state, and all excess energy is liberated in the form of heat, raising the temperature of the carrier gas. This locally increases the thermal decomposition of ^{3}Bi. Concheanainn and

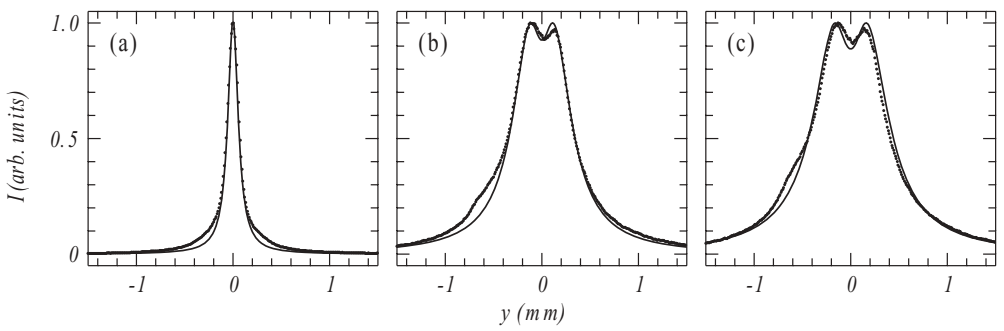

FIG. 6. Dots are measured line profiles in N_2 carrier gas at 1 bar, at time delays $t = 0$, 50, and 100 μs, for frames (a), (b), and (c), respectively. Full lines are computed profiles using Eqs. (4) and (5) and constants $n_0 = 2.4 \times 10^{13}$ m^{-1}, $k_1 = 672$ s^{-1}, $k_2 = 1.39 \times 10^{-15}$ s^{-1} m^{-3}, $k_3 = 0.1k_2$, and $D = 2 \times 10^{-5}$ m^2 s^{-1}.

Sidebottom report results on the decomposition of thermalized biacetyl triplets, which they, somewhat oxymoronically, call a "unimolecular pressure-dependent process" [37]. Relevant for our experiments is the temperature dependence of their "high-pressure limiting rate constant" $k_{\rm diss}$, $k_{\rm diss}(T) = 2 \times 10^{11} \exp(-7000/T)$, with T in K.

It turns out that the temperature rise of the carrier gas is too small to explain the enhanced decay of θ_B in the line center. Moreover, the observed dip hardly depends on the carrier gas (He, N_2, SF_6), while their heat capacity differs approximately by a factor 3.

In the second mechanism, one of the collision partners ends up in the ground state, while the other one dissociates into fragments. The dissociation products are assumed to be efficient collisional quenchers of ^{3}Bi, thus locally reducing the ^{3}Bi density. Highly internally excited biacetyl is likely to dissociate into two acetyl fragments, CH_3CO, with the excess energy raising the temperature. The quenching efficiency of the dissociation product (which could also be a secondary product, resulting from a chemical reaction of the primary dissociation product) is unknown, and treated as a free variable in the model presented below.

We assume that each triplet-triplet annihilation collision produces two radicals, and that these radicals, with concentration θ_R, are not consumed. This simple model results in the following equations for the concentrations:

$$\frac{\partial \theta_B}{\partial t} = -k_1\theta_B - k_2\theta_B^2 - k_3\theta_R\,\theta_B + D\nabla^2\theta_B, \qquad (4)$$

$$\frac{\partial \theta_R}{\partial t} = k_2\theta_B^2 + D\nabla^2\theta_R. \qquad (5)$$

The system of equations was solved numerically, with initial condition Eq. (3) and $\theta_R = 0$. The initial density n_0 was chosen such that $n_0 = 2.4 \times 10^{13}$ m^{-1}, while the rate constant $k_3 = 0.1k_2$ was chosen as best fit to the experimental intensity profiles. The computed profiles are shown in Fig. 6; they agree well with the line profiles measured in N_2 carrier gas at 1 bar, but in view of the choice of n_0 and k_3, this agreement can only be called qualitative.

The squared relative widths $\Delta^2(t)$ of the computed profiles are shown in Fig. 7, and are compared to the measurements. With our choice of n_0, the width of the model profile agrees

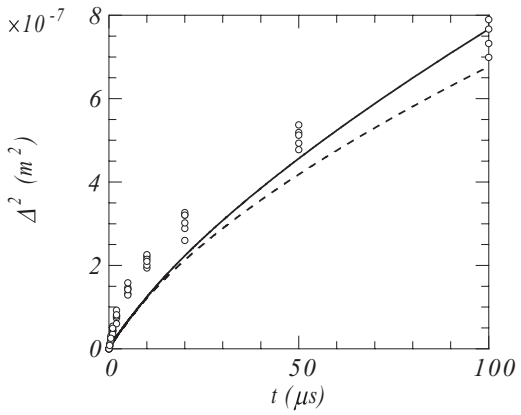

FIG. 7. Full line is the computed linewidth $\Delta^2(t)$ using Eqs. (4) and (5). Dashed line is the computed linewidth without molecular diffusion. The dots are the same data as in Fig. 5.

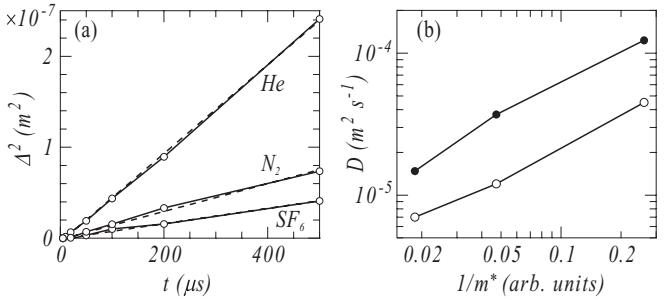

FIG. 8. Widening of lines of tagged biacetyl molecules at low laser pulse energy. (a) Open circles connected by full lines show Δ^2 measured in He, N_2, and SF_6 carrier gas; the dashed lines are fits $\Delta^2(t) = 16\ln(2)Dt$. (b) Open circles are measured diffusion coefficients, dots are diffusion coefficients computed from Eq. (6).

with the experiment at $t = 100\ \mu$s. We conclude that the overall time dependence of the model line shapes matches the experiment well.

Even at the very small pulse energies ($\approx 2\ \mu$J) of Fig. 5, the widening of the lines is almost completely determined by the triplet-triplet annihilation process, with a small effect of molecular diffusion. For even smaller pulse energies, the nonlinearity of biacetyl tagging is depleted and $\Delta^2(t)$ increases diffusively, as is illustrated in Fig. 8. The diffusion coefficients of excited triplet biacetyl molecules can be measured from the linear dependence on t of Δ^2 and have been compared to the simple hard-sphere coefficient for diffusion of biacetyl molecules into the carrier gas [38],

$$D_{12} = \frac{3}{8}\left(\frac{k_{\rm B}T}{2\pi m^*}\right)^{1/2} \frac{1}{n\,[(\sigma_1+\sigma_2)/2]^2}, \qquad (6)$$

where the index 1 points to biacetyl and 2 to the carrier gas, σ_1 and σ_2 are the molecular radii of the two gases, m^* is the reduced mass, $m^* = (m_1\,m_2)/(m_1+m_2)$, and where we ignored the contribution of self-diffusion of the dilute biacetyl gas to line widening. Little is known about the radius of the excited biacetyl molecule; we have used the value $\sigma_1 = 2.9 \times 10^{-10}$ m from Almy and Anderson [30]. Figure 8(b) illustrates that the measured and computed diffusion coefficients agree in their dependence on the reduced mass m^*, but all measured diffusion coefficients are a factor ≈ 2.5 smaller than the computed ones. It suggests that the radius of the excited biacetyl is approximately twice as large as was estimated in Ref. [30].

VII. CONCLUSION

The loss of accuracy due to broadening of written patterns is a serious problem of molecular tagging velocimetry. In fact, for tagged tracers with Schmidt number 1, when mass diffuses at the same rate as momentum, diffusional broadening poses a fundamental limit on the ability of MTV to resolve the smallest scales in turbulent flows of gases. Small-scale turbulent motion can only be resolved by using molecules which diffuse slower. Because of the emergence of the reduced mass m^* in the expression for the mutual diffusion coefficient [Eq. (6)] the size of these molecules is more important than their mass. Heavy molecular tracers may move slower, but their diffusion

in a light gas is determined by the mass of the light constituent. When $m_1/m_2 \gg 1$, $m_* = m_2$, and vice versa. Therefore, an arbitrarily small molecular diffusion of a tagged molecule can only be reached by increasing its diameter, not by increasing its mass.

Biacetyl is a relatively complex molecular tracer, which diffuses slower than the O_2 and NO molecular tracers of other techniques [1–5,8–11]. However, the accuracy of biacetyl tagging is not set by its diffusion, but by chemical reaction of the excited molecules. Due to nonlinear processes, the line widens much more quickly than through molecular diffusion. Of course, this is a function of the initial line profile; line widening is relatively rapid for the Lorentzian beam used in our experiment—it will be slower for Gaussian beams and will be absent for a perfect tophat profile, however, diffraction prohibits such a profile for narrow lines. We conclude that molecular tagging with biacetyl visualizes the large length scales of turbulence, much as for the other gaseous MTV techniques. Interestingly, excited biacetyl forms a model reactive system, which might be used to study the fundamental interaction between turbulence and chemical reaction.

ACKNOWLEDGMENTS

We gratefully acknowledge financial support by the "Nederlandse Organisatie voor Wetenschappelijk Onderzoek (NWO)" and "Stichting Fundamenteel Onderzoek der Materie (FOM)."

[1] M. M. Koochesfahani and D. G. Nocera, in *Handbook of Experimental Fluid Dynamics*, edited by J. Foss, C. Tropea, and A. Yarin (Springer-Verlag, Berlin, Heidelberg, 2007), Chap. 5.4, p. 362.
[2] R. B. Miles, C. Cohen, J. J. Conners, P. Howard, S. Huang, E. C. Markovitz, and G. Russell, Opt. Lett. **12**, 861 (1987).
[3] R. B. Miles, J. J. Conners, E. C. Markovitz, P. J. Howard, S. Huang, and G. J. Roth, Exp. Fluids **8**, 17 (1989).
[4] R. B. Miles, J. J. Conners, E. C. Markovitz, P. J. Howard, S. Huang, and G. J. Roth, Phys. Fluids A **1**, 389 (1989).
[5] A. Noullez, G. Wallace, W. Lempert, R. B. Miles, and U. Frisch, J. Fluid Mech. **339**, 287 (1997).
[6] C. Orlemann, C. Schulz, and J. Wolfrum, Chem. Phys. Lett. **307**, 15 (1999).
[7] S. Krüger and G. Grünefeld, Appl. Phys. B **69**, 509 (1999).
[8] N. J. Dam, R. J. H. Klein–Douwel, N. M. Sijtsema, and J. J. ter Meulen, Opt. Lett. **26**, 36 (2001).
[9] N. M. Sijtsema, N. J. Dam, R. J. H. Klein-Douwel, and J. J. ter Meulen, AIAA Pap. **40**, 1061 (2002).
[10] W. P. N. van der Laan, R. A. L. Tolboom, N. J. Dam, and J. J. ter Meulen, Exp. Fluids **34**, 531 (2003).
[11] J. Bominaar, M. Pashtrapanska, T. Elenbaas, N. Dam, H. ter Meulen, and W. van de Water, Phys. Rev. E **77**, 046312 (2008).
[12] A. H. Epstein, J. Eng. Power **99**, 460 (1977).
[13] B. Hiller, R. A. Booman, C. Hassa, and R. K. Hanson, Rev. Sci. Instrum. **55**, 1964 (1984).
[14] H. Hu and M. M. Koochesfahani, Exp. Fluids **33**, 202 (2002).
[15] B. Stier and M. M. Koochesfahani, Exp. Fluids **26**, 297 (1999).
[16] L. JianBang, P. Qi, L. ChangSheng, and S. JieRong, Acta Mech. Sin. **3**, 370 (1987).
[17] Z. Pikramenou, J. A. Yu, R. B. Lessard, A. Ponce, P. A. Wong, and D. G. Nocera, Coord Chem. Rev. **132**, 181 (1996).
[18] M. A. Mortellaro and D. G. Nocera, Chem. Tech. **26**, 17 (1962).
[19] D. G. Nocera, New Sci. **149**, 24 (1996).
[20] L. Mydlarski and Z. Warhaft, J. Fluid Mech. **320**, 331 (1996).
[21] W. Hwang and J. K. Eaton, Exp. Fluids **36**, 444 (2004).
[22] L. JianBang, P. Qi, L. ChangSheng, and S. JieRong, Exp. Fluids **6**, 505 (1988).
[23] J. Heicklen, J. Am. Chem. Soc. **81**, 3863 (1959).
[24] K. Eriks, T. D. Hayden, S. H. Yang, and I. Y. Chan, J. Am. Chem. Soc. **105**, 3940 (1983).
[25] M. E. Garabedian and D. A. Dows, J. Am. Chem. Soc. **90**, 2468 (1968).
[26] R. E. Rebbert and P. Ausloos, J. Am. Chem. Soc. **87**, 1847 (1965).
[27] H. W. Sidebottom, C. C. Badcock, J. G. Calvert, B. R. Rabe, and E. K. Damon, J. Am. Chem. Soc. **94**, 13 (1972).
[28] C. C. Badcock, H. W. Sidebottom, J. G. Calvert, B. R. Rabe, and E. K. Damon, J. Am. Chem. Soc. **94**, 19 (1972).
[29] R. L. McKenzie, D. J. Monson, and R. J. Exberger, Nasa Technical Memorandum, Report No. NASA-TM-78555, A-7720, Ames Research Center (1979).
[30] G. M. Almy and S. Anderson, J. Chem. Phys. **8**, 805 (1940).
[31] G. F. Sheats and W. A. Noyes, J. Am. Chem. Soc. **77**, 1421 (1955).
[32] W. A. Noyes, W. A. Mulac, and M. S. Matheson, J. Chem. Phys. **36**, 880 (1962).
[33] E. M. Thurlow and J. C. Klewicki, Phys. Fluids **12**, 865 (2000).
[34] R. B. Hill and J. C. Klewicki, Exp. Fluids **20**, 142 (1996).
[35] H. Okabe and W. A. Noyes, J. Am. Chem. Soc. **79**, 801 (1957).
[36] T. F. Hunter and M. G. Stock, J. Chem. Soc., Faraday Trans. 2 **70**, 1010 (1974).
[37] C. O. Concheanainn and H. W. Sidebottom, J. Photochem. **80**, 55 (1980).
[38] C. Chapman and T. G. Cowling, *The Mathematical Theory of Non-Uniform Gases* (Cambridge University Press, New York, 1939).